Materials Science-Poland, 30(3), 2012, pp. 282-289
http://www.materialsscience.pwr.wroc.pl/
DOI: 10.2478/s13536-012-0038-8

VERSITA

Microstructure and properties of ultrafine grain nickel 200 after hydrostatic extrusion processes

R. SITEK[1]*, C. KRAJEWSKI[1], J. KAMIŃSKI[1], M. SPYCHALSKI[1], H. GARBACZ[1], W. PACHLA[2], K. J. KURZYDŁOWSKI[1]

[1]Faculty of Materials Science and Engineering, Warsaw University of Technology, Woloska 141 Str., 02-507 Warsaw, Poland

[2]Institute of High Pressure Physics, Polish Academy of Science, Sokolowska 29/37 Str., 01-142 Warsaw, Poland

This paper presents the results of the studies of the structure and properties of ultrafine grained nickel 200 obtained by hydrostatic extrusion processes. Microstructure was characterized by means of optical microscopy and electron transmission microscopy. Corrosion resistance was studied by impedance and potentiodynamic methods using an AutoLab PGSTAT 100 potentiostat in 0.1 M Na_2SO_4 solution and in acidified (by addition of H_2SO_4) 0.1 M NaCl solution at pH = 4.2 at room temperature. Microhardness tests were also performed. The results showed that hydrostatic extrusion produces a heterogeneous, ultrafine-grained microstructure in nickel 200. The corrosive resistance tests showed that the grain refinement by hydrostatic extrusion is accompanied by a decreased corrosive resistance of nickel 200.

Keywords: *nickel 200, hydrostatic extrusion process, ultrafine grained microstructure, corrosive resistance*

1. Introduction

Material engineering contributed recently to the development of a novel group of materials with nanocrystalline structure, known as nanomaterials [1]. As unambiguously pointed out by literature data, materials of nanometric structure are characterized by better strength, thermal, chemical or biological properties compared to their microcrystalline equivalents which makes them suitable for different industry areas [1–6]. A disadvantage that limits a wider use of these materials is their lower plasticity (average ultimate elongation of titanium Grade 2 is ca. 15 % while the same materials with microcrystalline structure are characterized by ultimate extension of ca. 45 %), as well as a considerable uncertainty with regard to corrosion resistance. This uncertainty is based on the observation that nanomaterials are expected to exhibit a higher rate of diffusion due to the increased density of crystal defects. This results in an increased corrosion because of an accelerated intake of corrosive agents. However, one may also expect a faster formation of passive layers [7]. As suggested by the published data, the final balance might differ from material to material. Also, the corrosive resistance of the nanometals might depend on the environment, as demonstrated by the results obtained on nanocrystalline Ti [8–10].

Nanograined metals can be obtained by severe plastic deformation (SPD) methods, of which the most popular include equal channel angular pressing (ECAP), high pressure torsion (HPT) and hydrostatic extrusion (HE) [1, 11–18]. The last method, HE, was used in this study to refine the grain size in nickel 200. The resulting refined nickel was characterized in terms of the microhardness and corrosive resistance in: (a) 0.1 M Na_2SO_4 solution and (b) acidified (by addition of H_2SO_4) 0.1 M NaCl solution with pH = 4.2 at room temperature.

*E-mail: rsitek@inmat.pw.edu.pl

Table 1. Chemical composition of nickel 200 used in the present study.

Element	Ni	Cu	Fe	Mn	C	Si	S
Nickel 200	balance	0.5	6.0	1.0	0.15	0.5	0.015

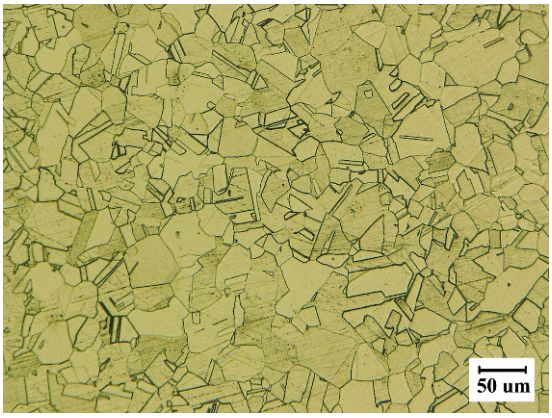

Fig. 1. The initial microstructure of nickel 200 revealed by metallographic methods.

2. Material and methods

The starting material was a nickel 200 rod with the diameter of 40 mm with chemical composition given in Table 1 and the microstructure presented in Fig. 1.

The supplied rods were cumulatively extruded with cooling at the exit of the die (except for the first run) into the diameters of: 6.92 mm and 4.94 mm with the maximum true strain of $\varepsilon = 4.2$.

Microstructure of the samples obtained by hydrostatic extrusion was investigated with a Jeol 300 kV electron transmission microscope. The effect of hydro-extrusion on the mechanical properties of the nickel was tested using a Hysitron TriboIndenter TI-900 device. Trapezoid course of the load was used in these tests, according to the scheme presented in Fig. 2.

Maximum load of 10 mN was used. During the test, the device was operated in a force feedback-control mode. Scanning Probe Microscopy (SPM) images of the surface were collected before the measurements.

Corrosion resistance was studied by impedance and potentiodynamic methods using an AutoLab PGSTAT 100 potentiostat in 0.1 M Na_2SO_4 solution and in acidified (by addition of H_2SO_4) 0.1 M NaCl solution at pH = 4.2 at room temperature. Impedance tests were conducted in a three-electrode system (test electrode – reference electrode: saturated calomel electrode [SCE] – auxiliary electrode [platinum]) in the frequency range of $10^5 - 10^{-3}$ Hz, and at the sinusoidal signal amplitude of 20 mV. Impedance spectra were analyzed using Boukamp's EQUIVCRT software. The obtained spectra were presented as Bode and Nyquist plots. Potentiodynamic tests were conducted in an identical three-electrode system up to the potential of 1500 mV. The material was polarized using potential scan rate of 0.2 mV/s. Macroscopic assessments of corrosive damage were performed using an Olympus SZX10 stereo microscope.

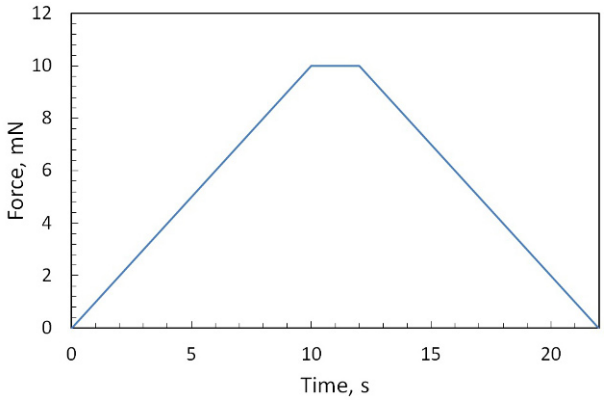

Fig. 2. Load vs. time curve used in the nano-hardness measurements.

3. Results

Fig. 3 presents electron microscopy images of the microstructure of nickel 200 subjected to hydrostatic extrusion process. It can be concluded that the extruded samples with the final diameter of φ = 6.95 mm are characterized by high grain refinement. The size of the grains ranges from nanometers to several micrometers, indicating also a high grain size heterogeneity and a presence of defects which might be due to localized plastic deformation.

After additional extrusion pass to the diameter of φ = 4.94 mm, further grain refinement was

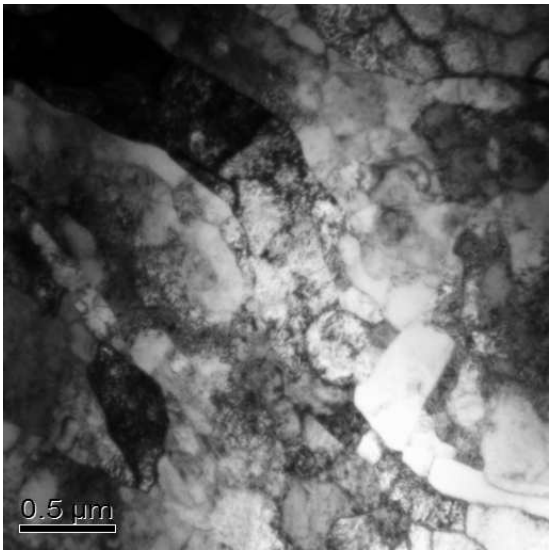

(a)

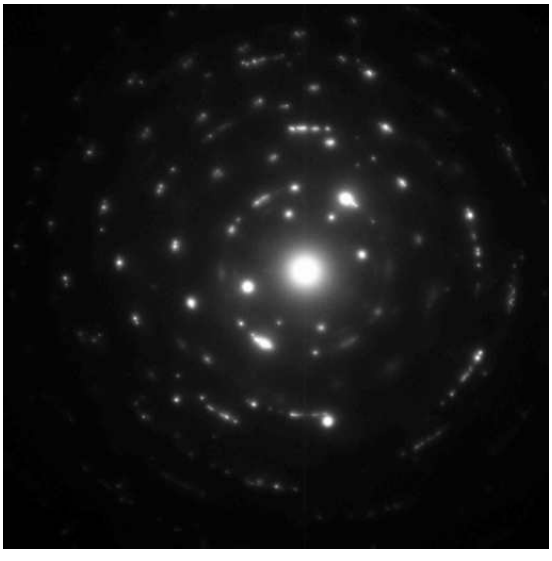

(b)

Fig. 3. Microstructure (a) and electron diffraction image (b) of nickel 200 after hydrostatic extrusion to the diameter of φ 6.95.

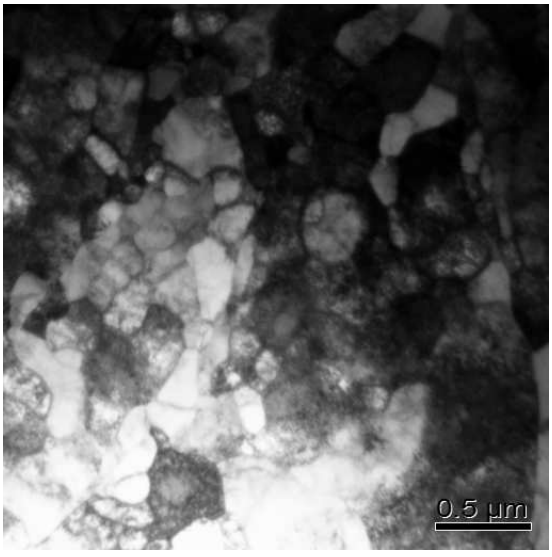

(a)

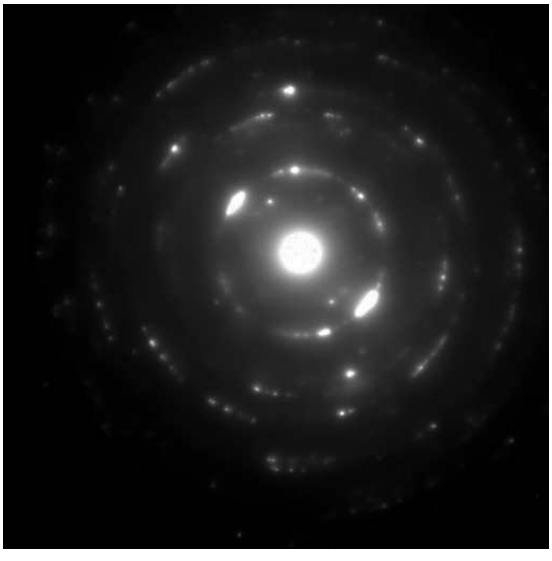

(b)

Fig. 4. Microstructure (a) and electron diffraction image (b) of nickel 200 after hydrostatic extrusion to the diameter of φ 4.94.

obtained with the average grain size of ca. 250 nm (Figs. 4 and 5). In these figures there are also visible the areas subjected to in situ recrystallization (Fig. 6) caused by the heat released during the extrusion due to the high pressures and very high deformation rate.

Fig. 7 presents the result of SPM imaging. The aim of the SPM studies was to determine the sample surface roughness. Results of these measurement are presented in Table 2. The average profile deviation from the average surface, R_a, is as low as 1 % of the average impression depth. Therefore, one may assume that the sample roughness has no impact on the measured hardness and Young's modulus.

In the hardness measurements 25 indentations were made in a square grid of 5 impressions per row and 5 impressions per column. Minimum

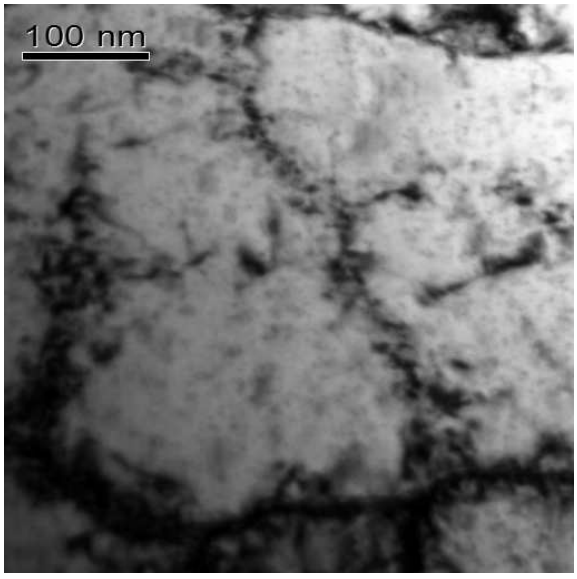

Fig. 5. Microstructure of nickel 200 after hydrostatic extrusion to the diameter of φ 4.94.

Table 2. Results of sample roughness measurements performed prior to nanohardness tests.

Area μm^2	R_a [nm]	R_q [nm]	Maximum height [nm]	Minimum height [nm]
100	2.8	3.7	13.5	-19.4

distance between the impressions was 30 µm. Berkovich diamond indenter was used. The obtained curves are shown in Fig. 8. High convergence of these curves provides an evidence of a low standard deviation. The hardness after hydro-extrusion was found to be 3.19 ± 0.12 GPa and the reduced Young's modulus 182 ± 5 GPa. Knowing the Poisson's numbers for nickel and diamond and the Young's modulus for diamond, the Young's modulus for the tested sample may be determined from Equation 1.

$$\frac{1}{E*} = \frac{(1-\nu^2)}{E} + \frac{(1-\nu'^2)}{E'}, \qquad (1)$$

where $E*$ is reduced Young's modulus, ν is Poisson's coefficient for the tested material (0.286), E is Young's modulus of the tested material, ν' is Poisson's coefficient for the indenter material (0.07), E' is Young's modulus of the indented material (1140 GPa).

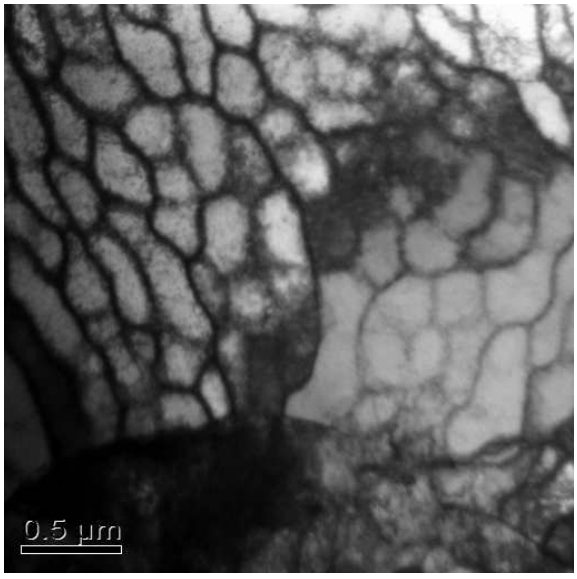

(a)

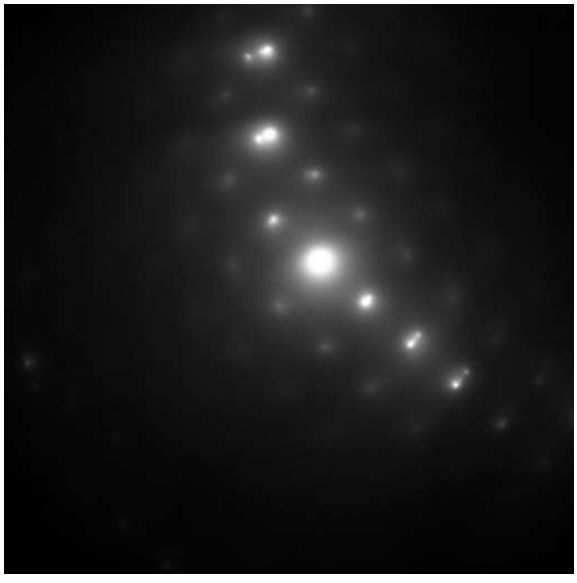

(b)

Fig. 6. Microstructure (a) and electron diffraction image (b) of nickel 200 after hydrostatic extrusion to the diameter of φ 4.94.

Poisson's number for nickel 200 used in the calculations was 0.286 [19], yielding the Young's modulus, determined from the equation, equal to 199 GPa.

For comparison, the hardness and Young's modulus of nickel 200 with coarse grain size were $1.83 \pm 0{,}05$ GPa and 205 GPa, respectively.

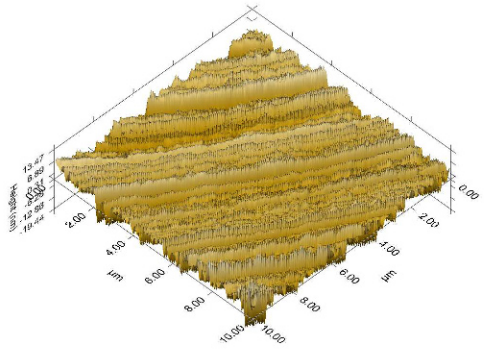

Fig. 7. The surface prior the measurement – SPM image.

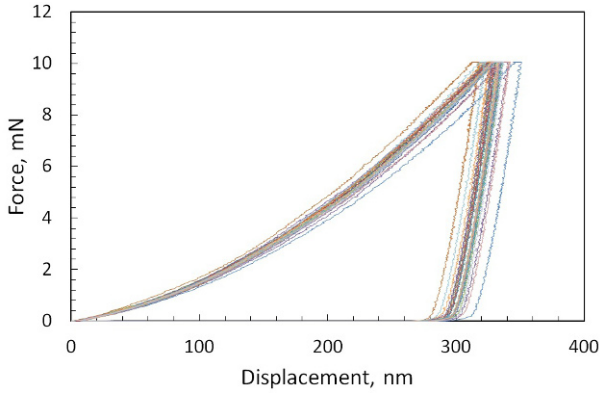

Fig. 8. Measured indentation curves.

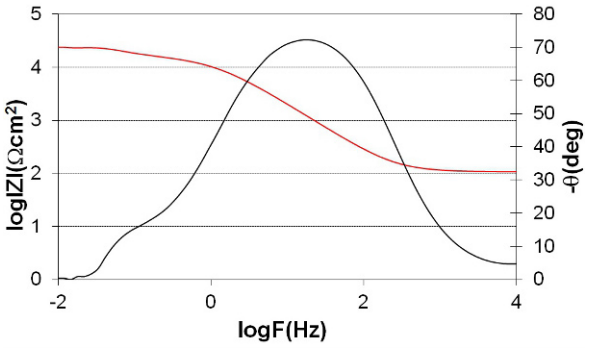

(a)

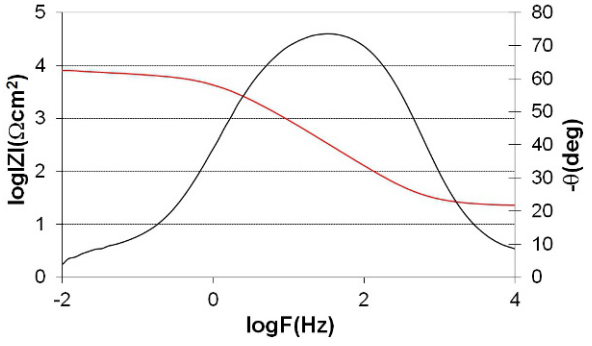

(b)

Fig. 9. Bode plots for the nickel 200: (a) initial structure, (b) after hydro-extrusion as exhibited in acidified 0.1 M NaCl.

The results of impedance tests of the nickel alloy as exhibited in acidified 0.1 M NaCl solution are presented in Fig. 9.

Two capacitance loops describing two electrochemical processes occurring on the material surface were identified. It may be assumed that these loops describe conditions within the pits and are characteristic of the passive layer. The obtained time constants suggest sensitivity of the hydro-extruded nickel to a local corrosion in the acidified sodium chloride environment. The calculated time constants of τ = ca. 0.1 s in both cases, are typical for intense electrochemical processes (such as pitting).

The analysis of the data in Table 3 revealed a reduction in corrosive resistance of the nickel alloy after hydrostatic extrusion. This is evidenced by both the reduction of R_t resistance from 14,300 Ωcm^2 to 5,900 Ωcm^2 and the increase in the capacitance of the passive layer from 7.53×10^{-6} F/cm^2 to 1.51×10^{-5} F/cm^2. The change in the passive layer capacitance is indicative of reduced thickness of the passive layer and thus of reduced stability of this layer in chloride-containing environments, which favors e.g. local corrosion.

Simultaneous potentiodynamic measurements (Fig. 10) confirmed the negative effect of hydroextrusion on the corrosion resistance of nickel in the environment of acidified sodium chloride solution.

The negative effect of hydroextrusion on the corrosion resistance is manifested by the increase in the density of corrosion currents from 2.5 $\mu A/cm^2$ to 4.5 $\mu A/cm^2$ and a reduction of the stability of the passive layer. Due to a high number

Table 3. Characteristic of electrochemical parameters of nickel alloy exhibited in chloride-containing environment.

Material		Pit area	Double coating
Nickel 200 (initial structure)	R (Ωcm^2)	7888	14300
	C (F/cm^2)	1.88E-04	7.53E-06
	n	1	0.9
Nickel 200 after hydro-extrusion process	R (Ωcm^2)	2458	5900
	C (F/cm^2)	1.30E-03	1.51E-05
	n	0.88	0.79

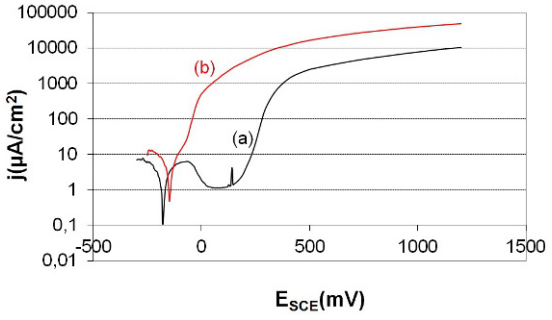

Fig. 10. Potentiodynamic curves of the nickel 200: (a) initial structure, (b) after hydroextrusion as exhibited in acidified sodium chloride solution.

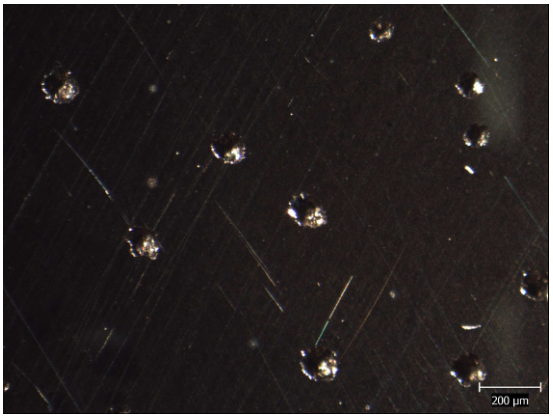

(a)

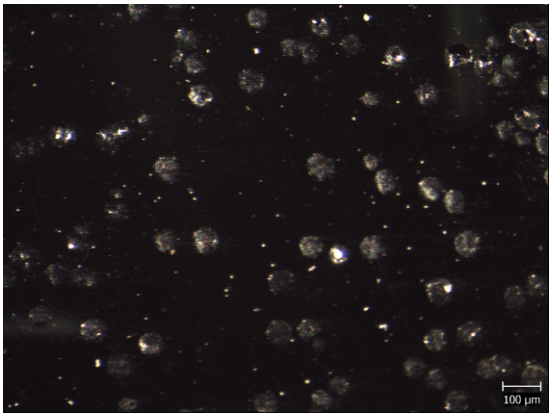

(b)

Fig. 11. Corrosion damage of nickel 200: (a) initial structure; (b) after hydro-extrusion – samples used for potentiodynamic measurements in acidified sodium chloride solution.

of pit nucleation sites (Fig. 11), the stability of the passive layer on the hydroextruded nickel alloy is low, as evidenced e.g. by a relatively low breakdown Enp = ca. -50 mV. In the case of the initial micro-grained alloy, the breakdown potential is Enp = ca. +200 mV.

Fig. 11 presents a corrosion pit in the as supplied micro-grained nickel alloy (Fig. 11a) and in the nickel processed by hydro-extrusion (Fig. 11b). The size of individual pits in both cases is comparable, but the intensity of pitting in the hydroextruded alloy is markedly higher.

Corrosion resistance of nickel alloys in sodium sulphate environment is much larger than in chloride-containing environment due to neutral pH of the solution and lack of chloride ions. Fig. 12 shows Bode plots for the nickel in initial state (a) and after processing by hydro-extrusion (b) as exhibited in the neutral sodium sulphate solution. The shape of impedance spectra suggests a single electrode process occurring at the material surface. The time constants determined for the process (τ = ca. 5 s, Table 4) indicate slight corrosion of the passive layer. High resistance of this layer is also indicated by high R_t values of 751,000 Ωcm^2 and 117,800 Ωcm^2 for the as-supplied nickel and after hydro-extrusion, respectively. The six-fold reduction in R_t value for the hydroextruded nickel suggests a negative impact of this process on the corrosion resistance. Double layer capacitances are comparable in both cases, which could indicate the stability of the passive layer on hydro-extruded nickel in sodium sulphate solution.

Simultaneous potentiodynamic measurements (Fig. 13) confirmed the negative effect of hydroextrusion on the corrosive resistance of

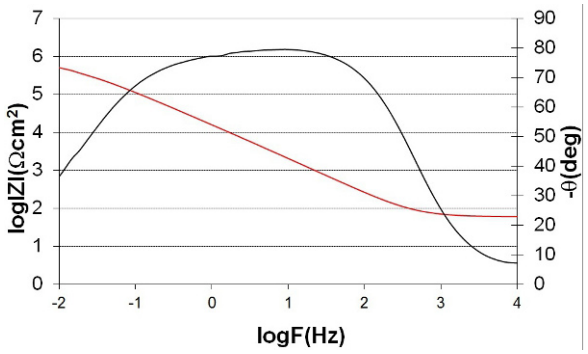

(a)

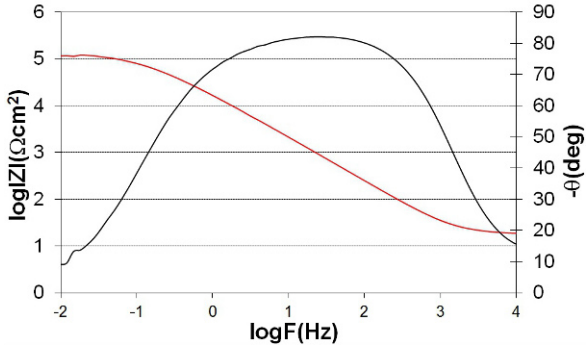

(b)

Fig. 12. Bode plots for nickel 200: (a) initial structure, (b) after hydroextrusion, as exhibited in 0.1 M Na_2SO_4.

Table 4. Characteristics of electrochemical parameters of nickel alloy exhibited in chloride-containing environment.

Material		Double coating
Nickel 200 (initial structure)	R (Ωcm^2)	751000
	C (F/cm^2)	8.25E-06
	n	0.89
Nickel 200 after hydroextrusion process	R (Ωcm^2)	117800
	C (F/cm^2)	7.2E-06
	n	0.91

nickel in the sodium sulphate environment. The corrosion current densities increased from 0.05 $\mu A/cm^2$ to 0.16 $\mu A/cm^2$ in the hydroextruded nickel alloy with constant corrosive potential value (E_{corr} = -160 mV $\pm$ 5 mV). The shape of potentiodynamic curves indicates that the micro- and nanocrystalline material exposed to sodium sulphate solution is in a passive state within the

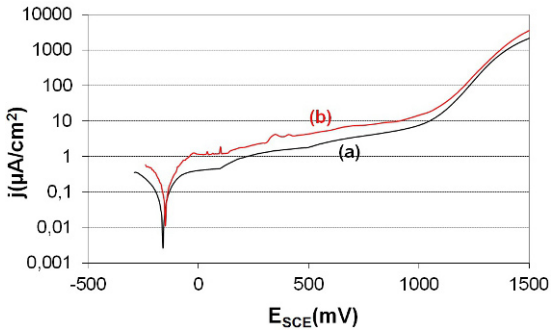

Fig. 13. Potentiodynamic curves of the nickel alloy: (a) initial structure, (b) after hydroextrusion as exhibited in sodium sulphate solution.

entire range of potentials tested. The observed increase in corrosion currents to above 1000 mV was caused by decomposition of water in the higher potentials range.

4. Conclusions

Following conclusions may be drawn from the obtained results:

The process of hydrostatic extrusion of a nickel 200 rod with microcrystalline structure leads to formation of heterogeneous, strongly defected, ultrafine-grain microstructure in entire extruded rod.

During the process, recrystallization takes place producing highly non-homogenous grain structure.

Nickel 200 with ultrafine grain structure is characterized by higher microhardness, but lower corrosive resistance in 0.1 M Na_2SO_4 solution and in acidified (by addition of H_2SO_4) 0.1 M NaCl solution at pH = 4.2 at room temperature as compared to nickel 200 characterized by microcrystalline structure.

Acknowledgements

The study was financed by the Ministry of Science and Higher Education as part of the N N507 274736 grant.

References

[1] KURZYDŁOWSKI K.J, LEWANDOWSKA M., Wydawnictwo Naukowe, PWN, Warszawa 2010 (in Polish).

[2] SERGUEEVA A.V., BRANAGAN D.J., MUKHERJEE A.K., *Mat Sci Eng A-Struct* 493 (1-2) (2008) 237.
[3] ZHILYAEV A.P., NURISLAMOVA G.V., V.ALIEV R.Z., BARO M.D., *Metall. Trans. 33A* (2002) 1865.
[4] ADAMCZYK-CIEŚLAK B., MIZERA J., KURZYDŁOWSKI K.J., *Inżynieria Materiałowa* 31 (3) (2010) 535.
[5] KOCH C.C., Nanostructured Materials - Processing, Properties, and Applications (2nd Edition) (2007) ISBN 978-0-8155-1534-0.
[6] VALIEV R., *Nature Mater.* 3 (8) (2004) 6
[7] KRÓLIKOWSKI A., *Ochrona przed Korozją* 50 (4) (2007) 140 (in Polish).
[8] GARBACZ H., *Inżynieria Materiałowa* 178 (3) (2010) 777.
[9] GARBACZ H., PISAREK M., KURZYDŁOWSKI KJ., *Biomol. Eng.* 24 (2004) 559.
[10] GARBACZ H., Prace Naukowe. Politechnika Warszawska. Inżynieria Materiałowa, (in Polish).
[11] PAKIEŁA Z. et al., *Nukleonika* 51 (1) (2006) 19.
[12] SKROTZKI W., TÓTH L.S., KLÖDEN B., BROKMEIER H.G., ARRUFFAT-MASSION R., *Acta Mat.* 56 (14) (2008) 3439.
[13] ZHANG H.W., HUANG X., PIPPAN R., HANSEN N., *Acta Mat.* 58 (6) (2010) 1698.
[14] VALIEV R.Z., SERGUEEVA A.V., MUKHERJEE A.K., *Scripta Materialia* 49 (2003) 669.
[15] LEWANDOWSKA M., KURZYDŁOWSKI K.J., *J. Mat. Sci.* 43 (23) (2008) 7299.
[16] VALIEV R.Z., LANGDON T.G., *Prog. Mat. Sci.* 51 (2006) 881.
[17] SAKAI G., HORITA Z., LANGDON T.G., *Mat. Sci. Eng. A* 393 (2005) 344.
[18] PACHLA W., KULCZYK, SUS-RYSZKOWSKA M., MAZUR A., KURZYDLOWSKI K.J., *J. Mat. Proc. Technol.* 205 (2008) 173.
[19] Product Reference Guide, Special Metals Corporation, 2000, Huntington, WV and H.M. Ledbetter, Cryogenics, v22, p 653, December (1982) and P.E. Armstrong and H.L. Brown, Trans. AIME, v230, p 962 (1964).

Received 2012-02-12
Accepted 2012-07-25